行政院原子能委員會

委託研究計劃研究報告

TomoDR 臨床前可用性測試研究

Investigation of the pre-clinical testing and usability assessment of TomoDR

計劃編號：1062001INER027

受委託機關(構)：林口長庚醫院

計劃主持人：陳建誠 醫師

聯絡電話：03-3281200 分機 3786

E-mail address：chenchiencheng@gmail.com

協同主持人：曾聖彬

研究期程：中華民國 106 年 6 月至 106 年 12 月

研究經費：新臺幣 507,600 元

核研所聯絡人員：廖英蘭

報告日期： 106 年 11 月 30 日

Content

TomoDR 臨床前可用性測試研究

計畫編號：1062001INER027

陳建誠、陳緯遠、黃怡璇

林口長庚醫院 影像診療科

中文摘要

行政院原子能委員會核能研究所(以下簡稱核研所)委託長庚醫院林口院區影像診療科，執行 106 年度「TomoDR 臨床前可用性測試研究」，目的為配合核研所自行開發放射造影儀「Taiwan TomoDR」數位斷層合成成像系統，探討斷層合成成像應用於放射診斷臨床檢查之可行性評估。

本計畫已完成五種常見臨床檢查條件之假體實驗，包含頭部、胸部、脊椎、手部與足部檢查。利用標準體型之類人型假體，於本院具斷層合成成像功能之數位放射攝影儀，醫事放射師依據臨床檢查條件選擇 X 光曝露參數，完成假體擺位與斷層合成攝影，影像品質與放射科醫師及醫學物理師進行討論，適當地調整檢查參數，以符合放射科醫師診斷之需求。假體完成攝影之影像已由放射科醫師完成影像雜訊量化分析，同時以五分法評估整體診斷影像品質。

本計畫已完成五種臨床常見檢查之參數最佳化，其影像品質符合臨床診斷需求，同時達到劑量合理抑低之目的，針對國際電工學會 IEC60601-1-6 Usability 報告，也提出數位斷層合成成像系統開發之建議，作為核研所開發 Taiwan TomoDR 之參考，也提供臨床前可行性評估之參考依據。

關鍵字：斷層合成成像、放射診斷學、影像品質、假體實驗

Investigation of the pre-clinical testing and usability assessment of TomoDR

Grant number 1062001INER027

Chien-Cheng Chen, Wei-Yuan Chen, Yi-Shuan Hwang

Department of Medical Imaging and Intervention, Chang Gung Memorial Hospital at Linkou, Taoyuan City 33302, Taiwan

Abstract

The department of medical imaging and intervention of Linkou Chang Gung Memorial Hospital was entrusted to investigate the study "Pre-clinical testing and usability assessment of TomoDR" from Institute of Nuclear Energy Research (INER). The purpose of this study was to investigate the X-ray tomosynthesis in application to medical imaging of diagnostic radiology.

The image quality and radiation dose of the five common protocols in routine examination (head, chest, spine, hand, and foot) were evaluated with a standard-sized phantom in a digital X-ray tomosynthesis in our department. The phantom was positioned by a radiological technologist according to the imaging technique guidance. The imaging parameters of each protocol was suggested by a radiologist and a medical physicist based on diagnosis requirement. The phantom image noise was quantified and the diagnostic image quality was determined with a five-grade system by a radiologist.

The five routine protocols were optimized in this study. The image quality has been adjusted to meet the diagnosis requirement and the ALARA (as low as reasonably achievable) principle. Based on our study, we provided a suggestion according to the report of IEC 60601-1-6 Usability for the development of digital X-ray tomosynthesis (Taiwan TomoDR) to INER.

Keywords: tomosynthesis; diagnostic radiology; image quality; phantom study

I. Research motivation

The Chang Gung Memorial Hospital (CGMH) was established in 1976 and played the role as a mediating center that introduced modern medical knowledges and technologies from around the world to Taiwan in the early periods of its establishment. CG MH now is a world class medical center and has six branches in Taiwan (Figure 1). The Linkou Branch of CGMH serves the largest number of beds in the nation. The number of employee is more than 6,000. Our hospital sees an annual average of two billion outpatients, two hundred thousand patients in the emergency department, and handle about one hundred thousand patients that have sought surgery or hospitalization.

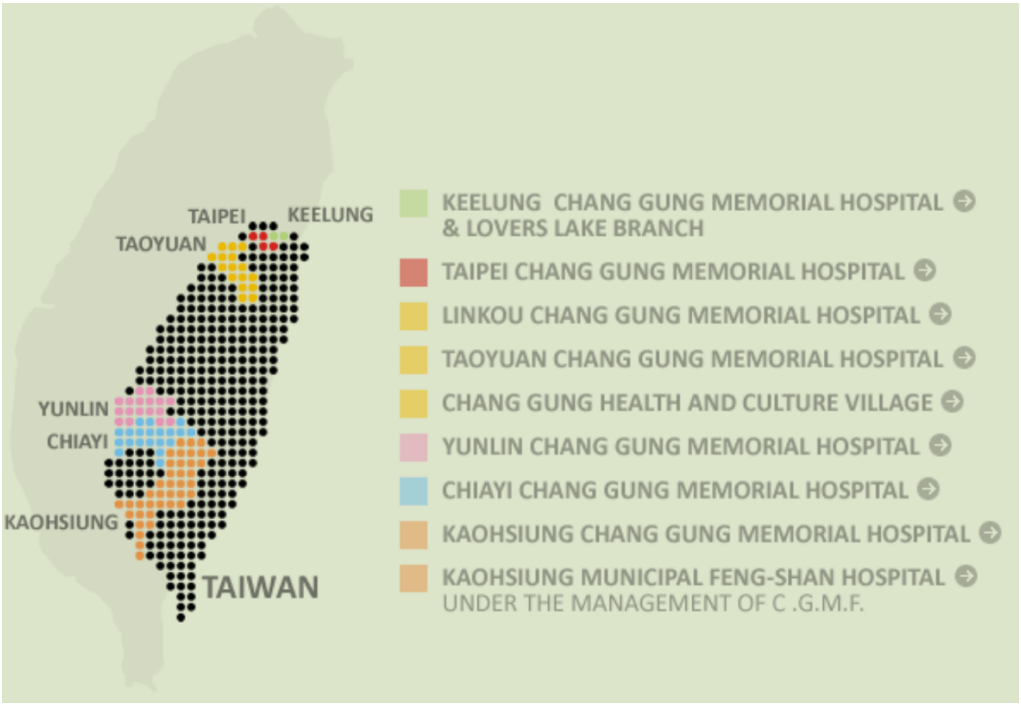

Figure 1: CGMH location in Taiwan.

Department of Medical Imaging and Interventions provides the clinical services in hospital at Linkou, Taipei, and Taoyuan. We have

four divisions in Linkou branch. There are gastro-intestinal, neuroradiology and emergency radiology. Our services are customer-oriented and based on the patient-centered policy. The Department is equipped with 20 conventional radiographic units, 24 portable X-ray units, 7 fluoroscopic units, 9 computed tomography (CT) machines, 5 ultrasonographic scanners, 5 magnetic resonance imaging (MRI) scanners, 1 car-mobile X-ray unit, 3 bone marrow densitometer systems and 2 digital mammographic units.

INER has invited the PI and his research team to investigate the clinical application with digital X-ray tomosynthesis. The purpose of this study was to investigate the diagnostic image quality and radiation dose in application to different clinical situation with phantom study. The recommendation of IEC 60601-1-6 Usability was provided in this report as well. A medical physicist, a radiological technologist, and an radiologist were included in our research team.

II. Materials and methods

1. Digital tomosynthesis technique development in diagnostic radiology

There are three X-ray digital tomosynthesis modalities as showed in Figure 2 in our department (Safire, SONIALIVISION, Shimadzu, Japan). The X-ray machine could be used for a wide variety of examination and treatment procedures, such as upper gastro-intestinal intervention (GI) screening, endoscopic retrograde cholangiopancreatography (ERCP), pre- and post-operative contrast radiography for gastro-intestinal surgery, bronchoscopy for respiratory medicine, hysterosalpingography (HSG) for gynecology, myelography and arthography for orthopedics, and VF (video fluoroscopy) for oral surgery.

Tomosynthesis was not planned for routinely used and only valid for extra request from medical doctors for further investigation and diagnosis. Figure 3 to Figure 5 showed one of our X-ray digital tomosynthesis machine, the remote-control system, and the image processing work station.

Figure 2: The X-ray machine in our department was manufactured by Shimadzu. The photographic demonstrates a patient examination with radiography and fluoroscopy.

Figure 3: Shimadzu X-ray digital X-ray digital radiography, fluoroscopy, and tomosynthesis.

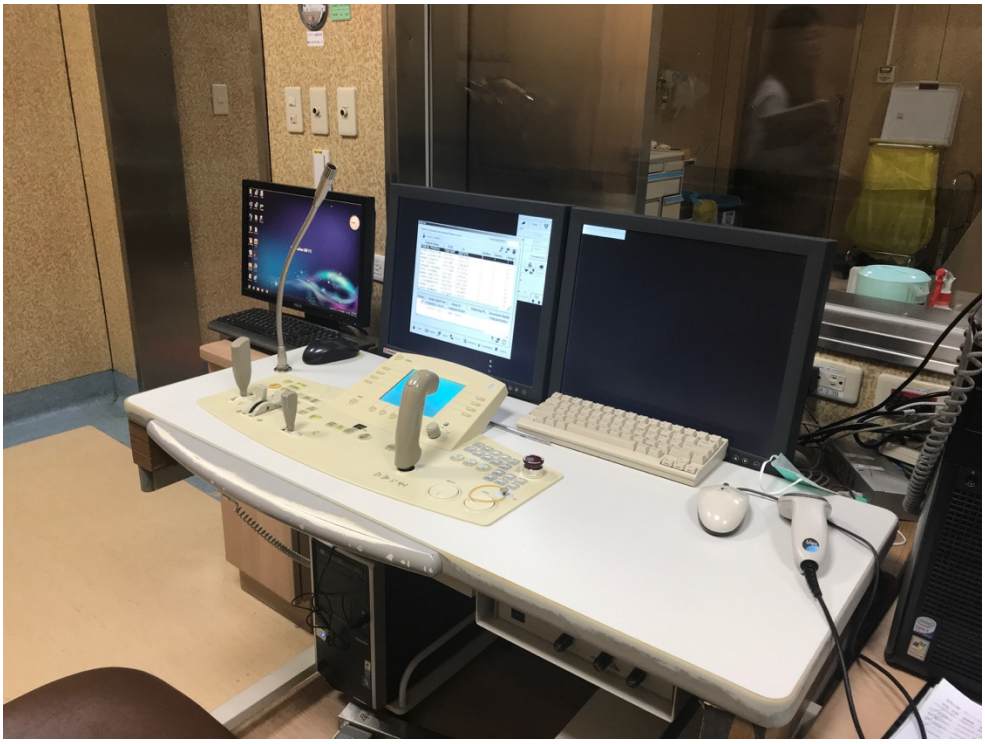

Figure 4: Remote-control station of the X-ray digital radiography, fluoroscopy, and tomosynthesis.

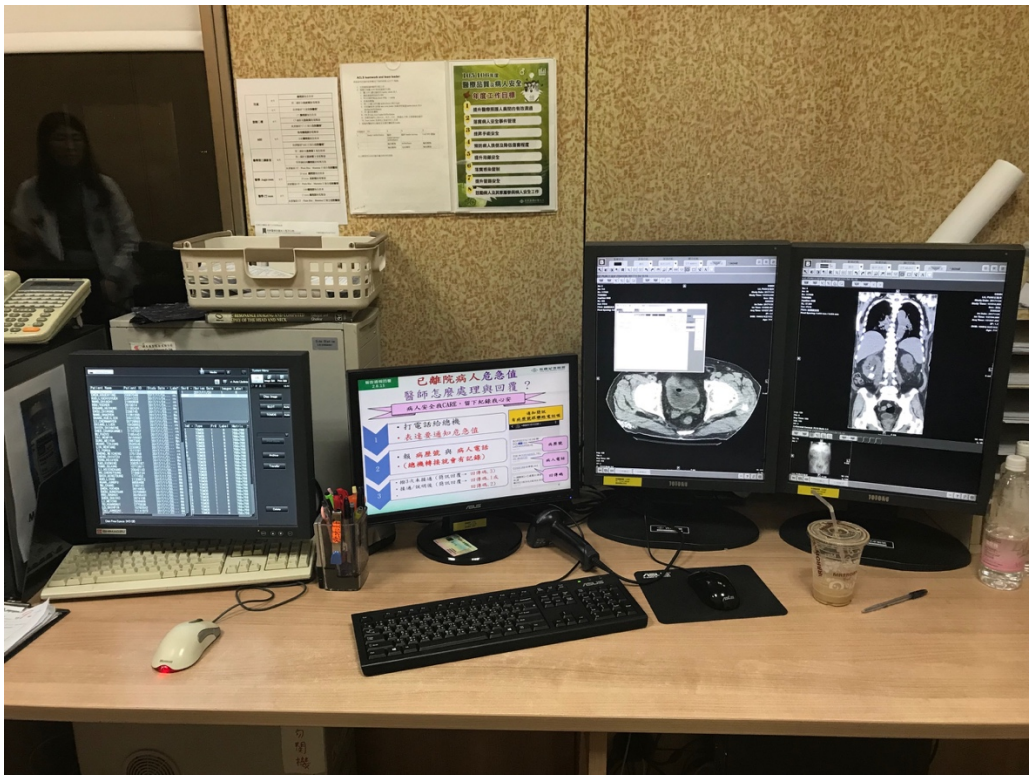

Figure 5: Image post-processing work station of the X-ray digital radiography, fluoroscopy, and tomosynthesis.

2. X-ray tomosynthesis of adult routine protocols

Figure 6 showed an average-sized anthropomorphic phantom (KYOTO KAGAKU, Japan) which was used to perform the chest examination. Five adult routine examinations using the digital X-ray tomosynthesis machine were assessed in this study. Those examinations were head, chest, thorax-to-lumbar spine (T-L spine), hand, and foot. The imaging acquisition parameters for those examinations recommended by the manufacture were listed in Table 1. The radiological technologist used pulsed fluoroscopy to determine the imaging field of view (FOV) and then selected a protocol.

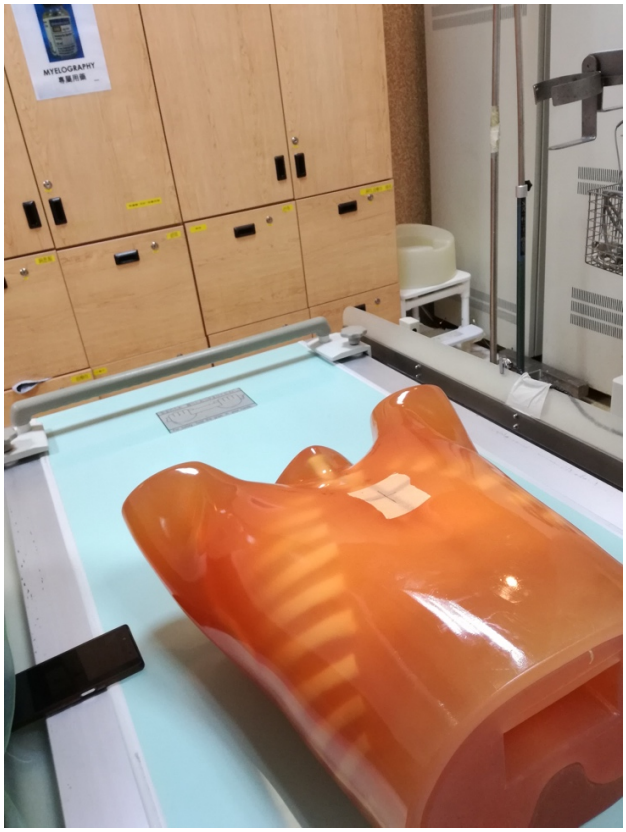

Figure 6: An adult chest region phantom underwent a chest X-ray tomosynthesis.

Table 1: Imaging acquisition parameters recommended by the manufacture for tomosynthesis.

Protocol	**Head AP**	**Head Lateral**	**Chest AP**	**T-L spine AP**	**T-L spine Lateral**	**Hand AP**	**Hand Lateral**	**Foot AP**	**Foot Lateral**
Tube voltage (kVp)	87	87	120	80	80	57	57	70	70
Tube current (mA)	500	500	250	320	320	250	250	250	250
Exposure time (ms)	10	10	3.2	16	16	10	10	14	14
Angular range (deg)	±20	±20	±20	±20	±20	±20	±20	±20	±20
Number of projections	74	74	74	74	74	74	74	74	74
Center of depth (mm)	100	100	100	75	150	40	40	80	80
Source to detector distance (cm)	110	110	110	110	110	110	110	110	110
Reconstructed slice thickness (mm)	1	1	5	2	2	1	1	1	1
Reconstructed algorithm (SA, FBP)*	FBP	FBP	FBP	FBP	FBP	FBP	FBP	FBP	FBP

* FBP: filtered-back projection algorithm.

* SA: shift-and add algorithm.

3. Experimental setup and phantom part position

Figure 7 showed the head examination. The basic position and it center ray followed the radiography positioning instruction (Figure 8) and the X-ray tube will move along with the longitudinal axis (cranial-to-caudal direction). The phantom position and its detailed position instruction and the central ray for the other four protocols was showed in Figure 8 to Figure 11 and Figure 13 to Figure 18. Before X-ray tomosynthesis examination, the FOV was determined using the pulsed fluoroscopy mode. The radiological technologist will perform all the imaging procedure. After the image acquisition, the image slices would be transformed from the imaging station to the post-processing image work station. The number of slice for tomosynthesis examination was huge and it took one hour for all the post processing procedure.

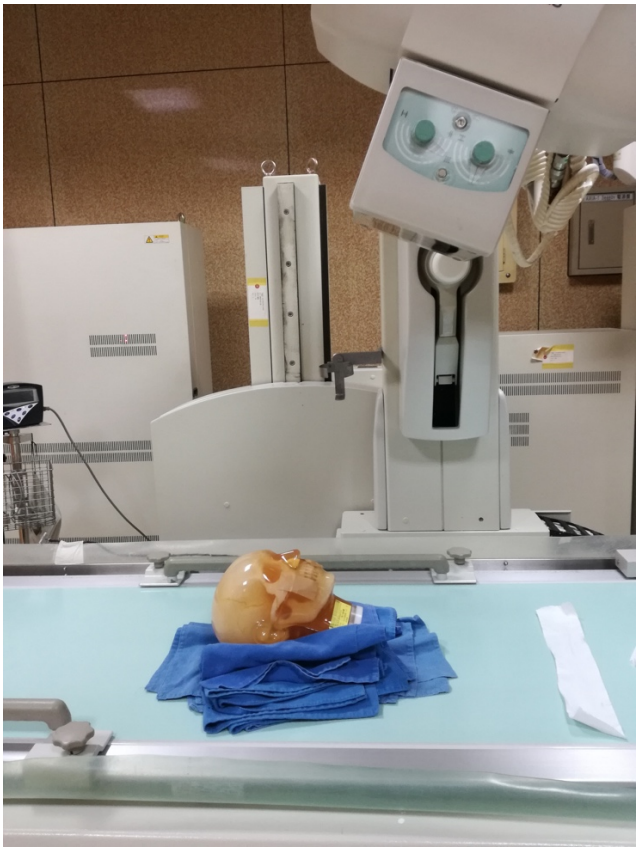

Figure 7: Experiment setup and Kyoto Kagaku head phantom (PH-47).

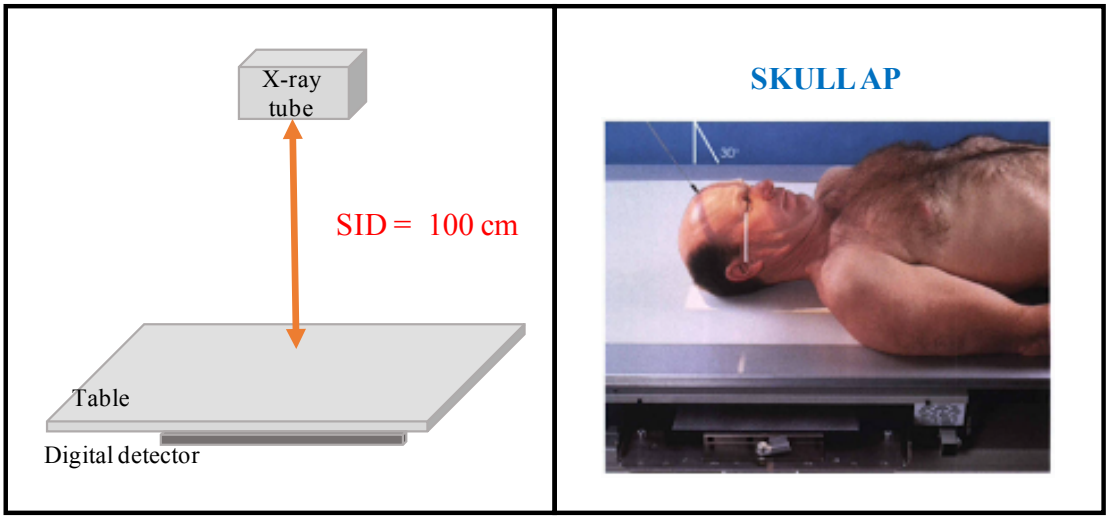

SKULL AP

① Remove all metallic or plastic objects from patient's head and neck.
② Exposure taken with patient in the supine position.
③ Central ray is perpendicular to IR (parallel to OML) and is centered to exit at gabella.

Figure 8: Skull AP view

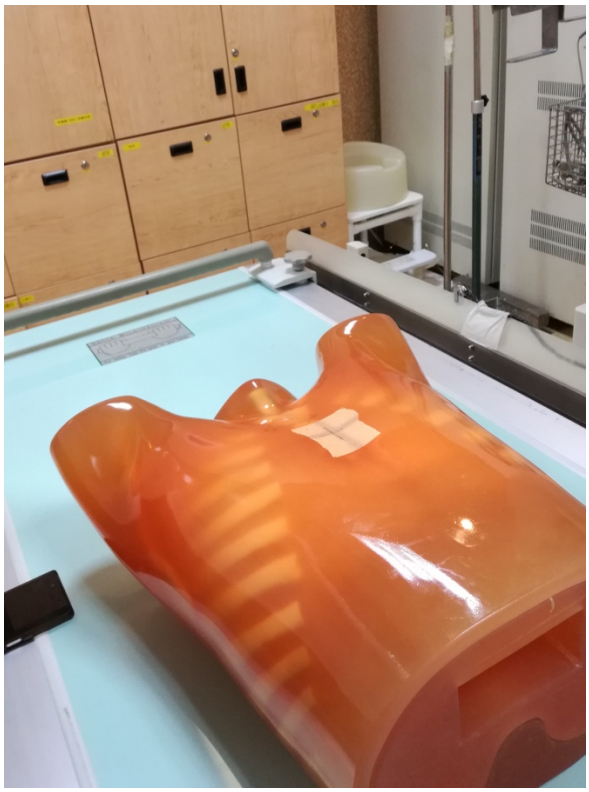

Figure 9: Experiment setup and Kyoto Kagaku chest phantom (N1).

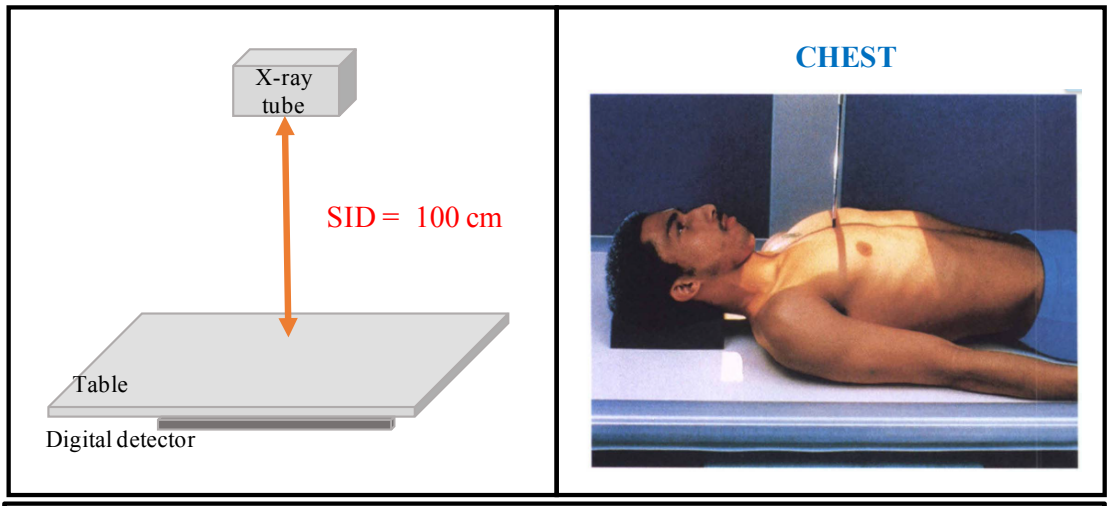

CHEST

① Patient is supine,
② If possible, the head end of the cart or bed should be raised into a semierect position.
③ Roll patient's shoulders forward by rotating arms medially or internally.
④ Central ray to level of T7, 3 to 4 inches (8 to 10cm) below jugular notch.

Figure 10: Chest view

Figure 11: Experiment setup and Kyoto Kagaku torso phantom (CTU-41).

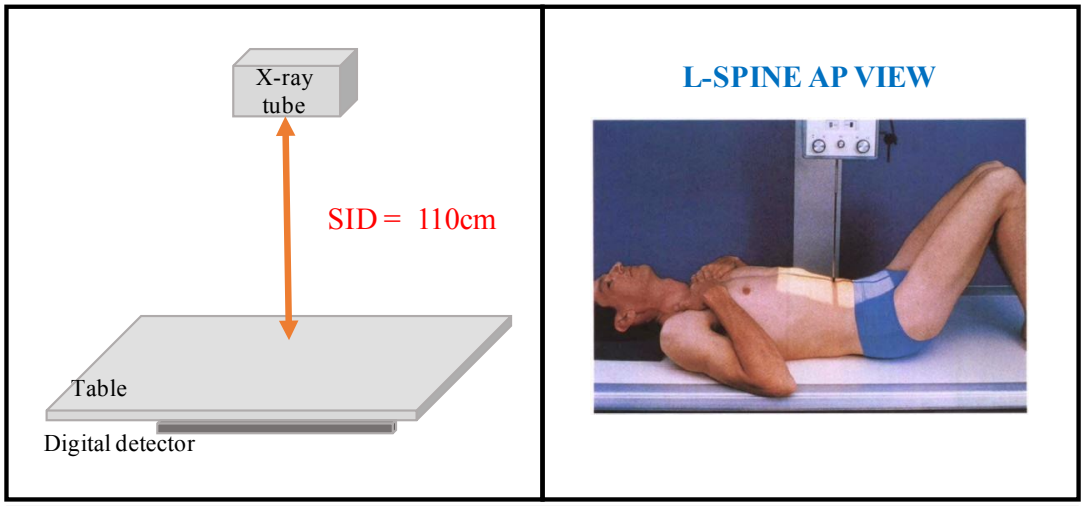

L-SPINE AP VIEW

① Let patient in supine and slightly flex the knee and put pillow on head for patient comfortability.
② Midsagital plane is align to central ray and in the midline of table or bucky.
③ Put arm on chest or at the side.
④ Ensure that no rotation of torso or pelvis exist.
⑤ Center to level of illiac crest between L4-L5 interspace. This large image receptor will include the lumbar vetebrae, sacrum, and possibly coccyx.

Figure 12: Radiography position instruction of L-spine AP view

Figure 13: Experiment setup and Kyoto Kagaku hand phantom (Optional part of PH-2/2B).

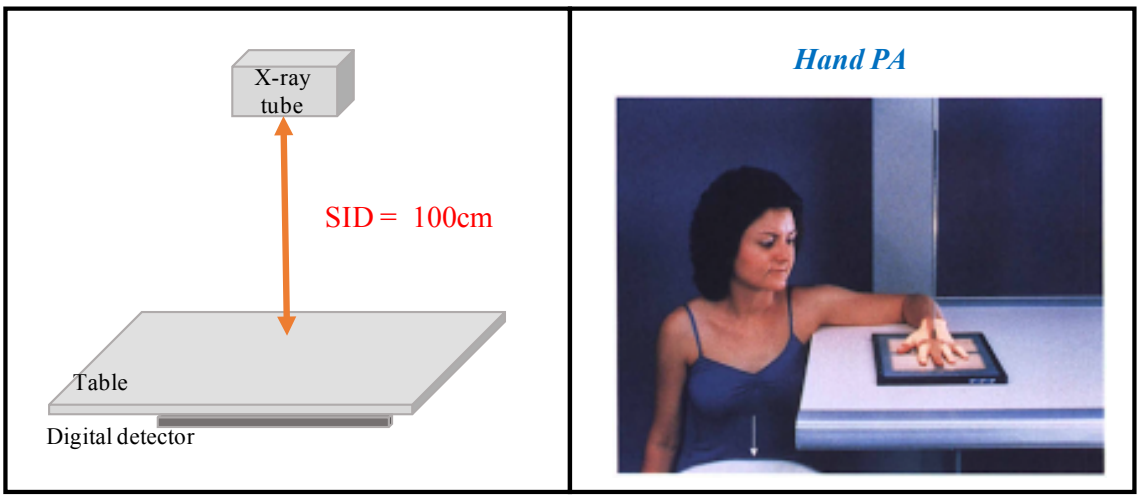

Hand PA

① Seat patient at of table with elbow flexed about 90 degrees and hand and forearm resting on table.

② CR perpendicular to IR, directed to third MCP joint.

Figure 14: Radiography position instruction of Hand AP view

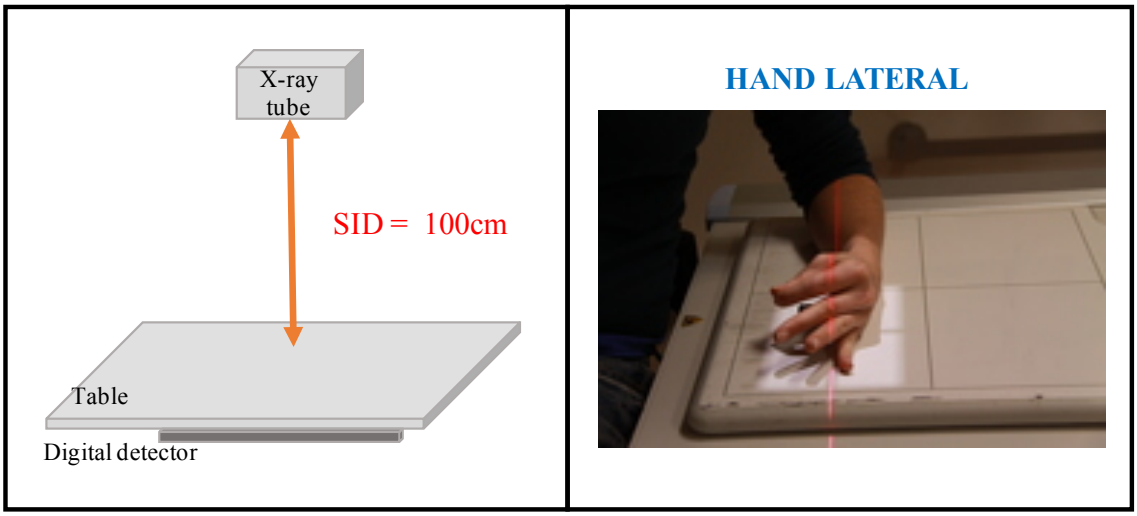

HAND LATERAL

① Patient is seated alongside the table

② Hand is externally rotated by 90 degrees from the PA position so that the palm is perpendicular to the image receptor

③ Fingers are kept extended with thumb abducted

④ Fingers should ideally be separated to minimize superimposition and increase diagnostic information contained in the image

Figure 15: Radiography position instruction of Hand Lateral view

Figure 16: Experiment setup and Kyoto Kagaku foot phantom (Optional part of PH-2/2B).

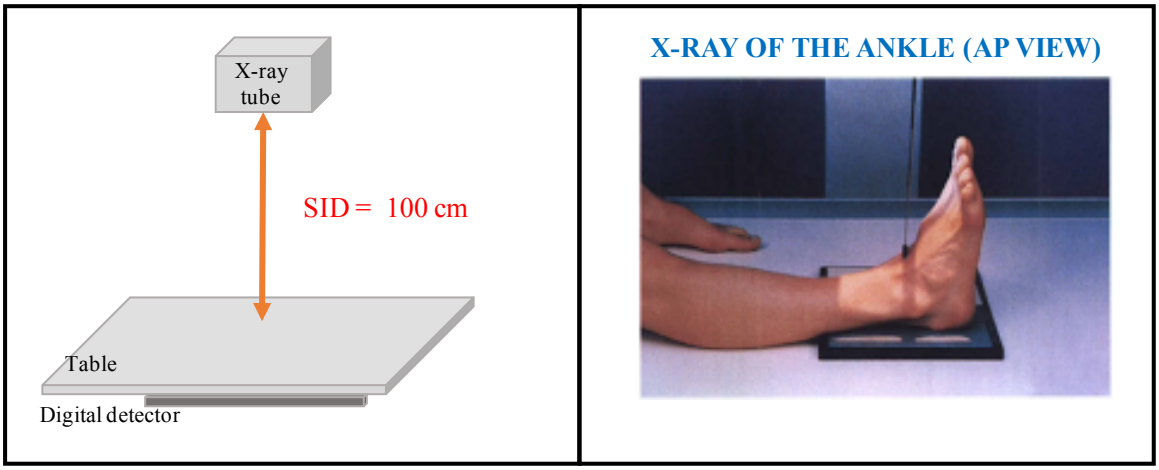

X-RAY OF THE ANKLE (AP VIEW)

① Center and align ankle joint to CR and to long axis of portion of IR being exposed.
② Do not force dorsiflexion of the foot but allow it to remain in its natural position.
③ Adjust the foot and ankle for a true AP projection. Ensure that the entire lower leg is not rotated. The intermalleolar line will not be parallel to IR.
④ Take radiograph with patient in the supine position; place pillow under head; patient's leg should be fully extended.

Figure 17: Radiography position instruction of Ankle AP view

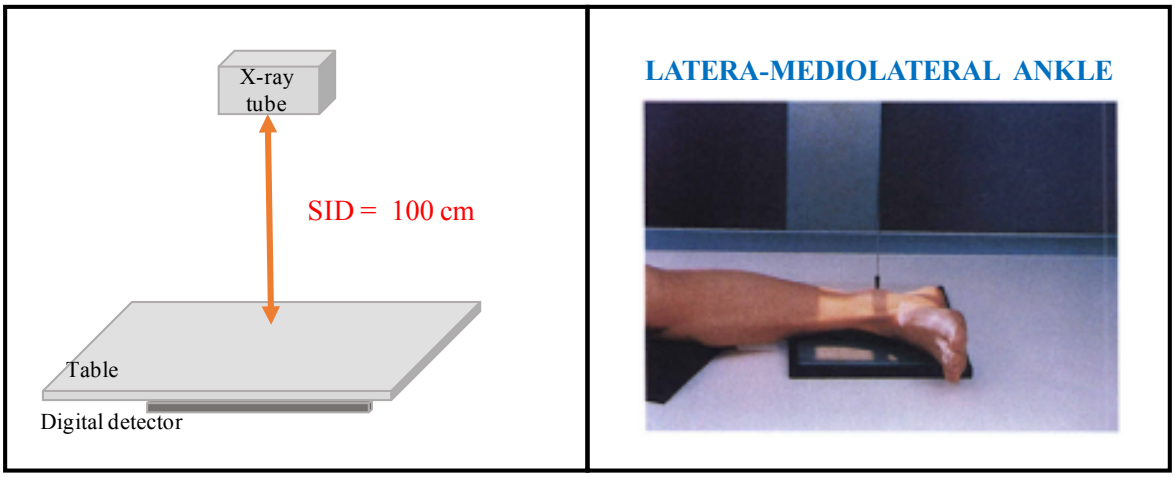

LATERA-MEDIOLATERAL ANKLE

① Place patient in the lateral recumbent position, affected side down;
② Give pillow for head; flex of affected limb about 45 degree;
③ Place opposite leg behind the injured limb to prevent over-rotation.
④ CR perpendicular to IR, directed to medial malleolus.

Figure 18: Radiography position instruction of Ankle Lateral view

4. Imaging parameter adjustment

Those five routine protocols were recommended from X-ray scanner manufacture. The imaging parameters showed in Table 2 were adjusted according to the radiologist and medical physics recommendation. The results of the image quality were assessed by the radiologist as well.

Table 2: Adjustment of imaging parameters of the five protocols.

Protocol	**Adjustment of imaging parameters**
Head	
Adjustment 1	Reconstructed slice thickness 2 mm
Chest	
Adjustment 1	Reconstruction algorithm of FBP, 100 kVp
T-L Spine	
Adjustment 1	86 kVp, 500 mA, 2 ms
Hand	
Adjustment 1	50 kVp, 3.2 ms
Adjustment 2 (AP view)	62 kVp
Foot	
Adjustment 1	60 kVp, 2.8 ms
Adjustment 2	80 kVp
Adjustment 3	60 kVp, 2.8 ms, reconstructed slice thickness 2 mm
Adjustment 4	75 kVp
Adjustment 5 (Lateral view)	60 kVp, 2.8 ms, reconstructed slice thickness 2 mm

5. Quantitative and Qualitative Image Quality Evaluation

Image noise measurement was used to represent the quantitative image quality. The region of interest (ROI) was defined by the radiologist located at uniform tissue, such as muscle and fat. The measured standard deviation of the ROI was used to described the image noise. The phantom images quality was graded by a senior radiologist (more than 10-year experience) blinded to all the imaging parameters. The visualization of these part was graded from one to five (One: not visualized; Two: moderate visualization; Three: good visualization; Four: very good visualization; Five: excellent visualization). For visualization of image artifacts, the significant image artifact was marked by the radiologist when reviewing all the images.

6. Organ dose and effective evaluation

The organ doses were measured with thermoluminescent dosimeter (TLD). The TLD chips were inserted into specified organs location (esophagus, lung, stomach, liver, gonads, skin, and thyroid). The effective doses for each protocol were calculated according to ICRP recommendation.

Table 3: Five grade method for visualization of image quality

Grade	Image characteristics
1	(1) Tissue and organ could not be separately visualized with server overlapping. Lack of diagnosis information. (2) Server image artifact, impacting diagnosis for the lesion or target region. (3) insufficient image contrast resolution, impacting diagnosis for the lesion or target region.
2	(1) Tissue and organ might be separately visualized with moderate overlapping. Little diagnosis information. (2) Moderate image artifact, impacting part of diagnosis for the lesion or target region. (3) Less image contrast resolution, impacting part of diagnosis for the lesion or target region.
3	(1) Tissue and organ could be separately visualized with acceptable overlapping. Diagnosis information is enough and acceptable. (2) Mild image artifact, no impact on diagnosis for the lesion or target region. (3) Acceptable image contrast resolution, no impact on diagnosis for the lesion or target region.
4	(1) Tissue and organ could be separately visualized without overlapping. Diagnosis information is enough and acceptable. (2) Less image artifact, no impact on diagnosis for the lesion or target region. (3) Detailed image contrast resolution, no impact on diagnosis for the lesion or target region.
5	(1) Tissue and organ could be separately visualized without overlapping. Diagnosis information is excellent. (2) Acceptable image artifact, no impact on diagnosis for the lesion or target region. (3) Excellent image contrast resolution, no impact on diagnosis for the lesion or target region.

III. Results and discussion

1. 2D radiographic and tomosynthesis image

Figure 19 showed the anterior-to posterior (AP) view of head tomosynthesis image. The nasal cavity and the maxillary sinus could be clearly visualized as the yellow arrows indicated. The overall image contrast is good and the image artifact is not appeared in the diagnosis region.

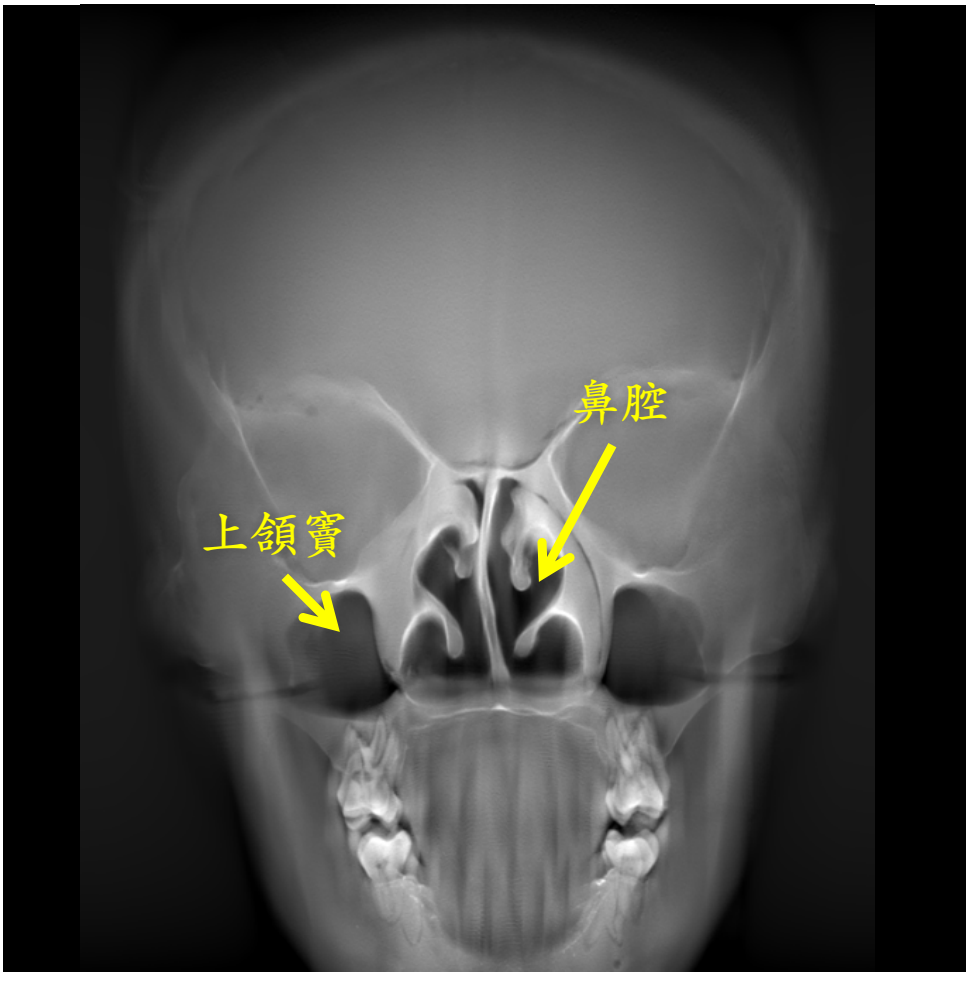

Figure 19: Phantom image (Skull AP view)

Figure 20 showed the lateral view of head tomosynthesis image. The temporal bone, temporalmandibular (TM) joint, and the mandibular bone could be clearly visualized as the yellow arrows indicated. The overall image contrast is good and the image artifact is not appeared in the diagnosis region.

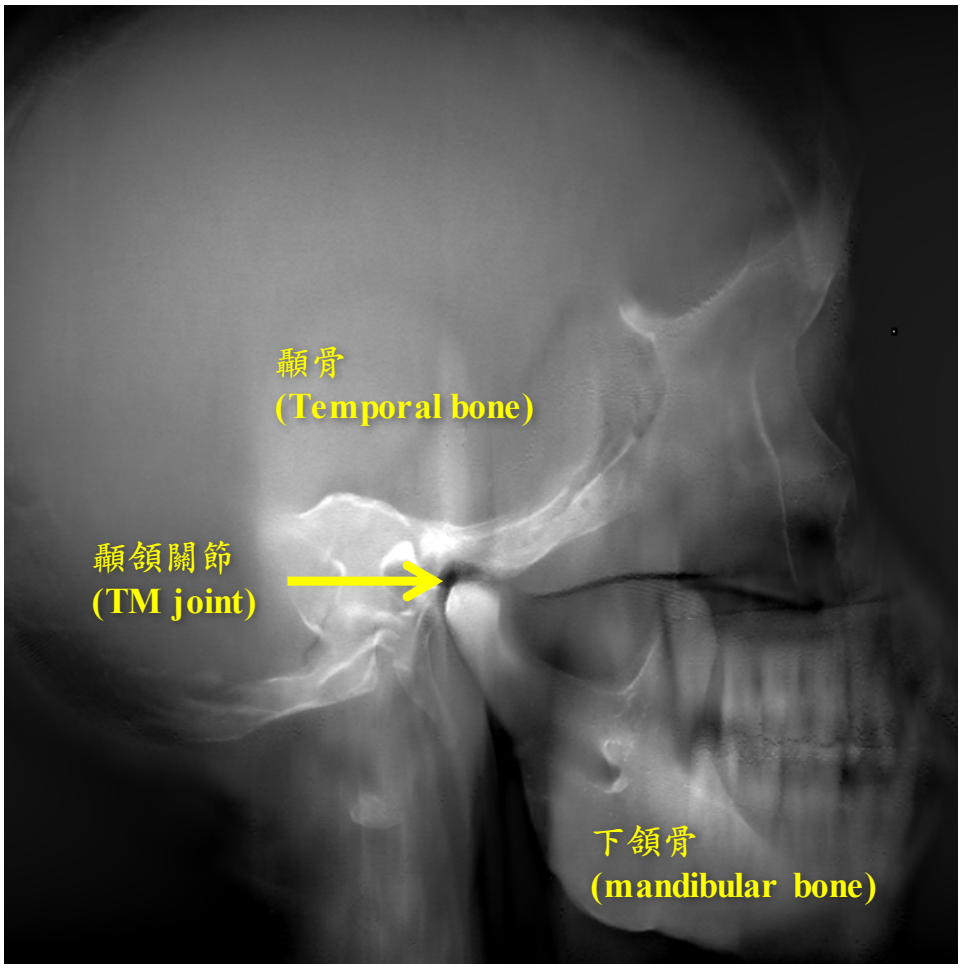

Figure 20: Phantom image (Skull Lateral view)

Figure 21 showed the AP view of chest tomosynthesis image. The aortic arch, left- and right-side bronchus could be clearly visualized. The tumor mimic objects with diameter of 2, 3, 5, 8 mm inserted into the lung region could be well visualized as the yellow arrows indicated. All the boundary of those objects could be clearly defined. The overall image contrast is good and the image artifact is not appeared in the diagnosis region.

In Chou et al. suggestion, gigital tomosynthesis of the chest is similar to digital radiography, but that also provides some of the benefts of computed tomography (CT). The major advantages of DTS over conventional chest radiography are improved visibility of the pulmonary parenchyma and depiction of abnormalities such as pulmonary nodules. Calcifcations, vessels, airways, and chest wall abnormalities are also much more readily visualized at DTS than at chest radiography.

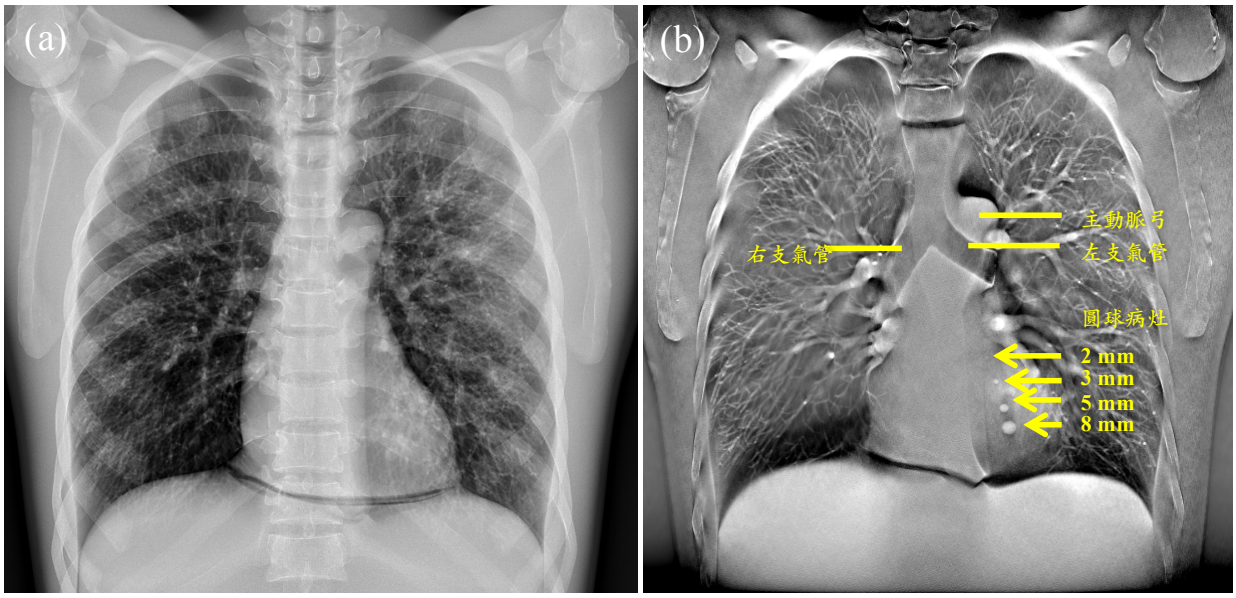

Figure 21: Phantom image (Chest AP view)

Figure 22 showed the AP view of T-L spine tomosynthesis image. The tomosynthesis image (Figure 22 b) provides excellent image quality in bony structure discrimination and image resolution compared with the conventional digital radiography (DR) (Figure 22 a). The spine detailed information at each depth could be visualized while the DR image showed the tissue superimposition and poor image resolution. The pedicle, facet joint could be clearly visualized. The overall image contrast is good and the image artifact is not appeared in the diagnosis region.

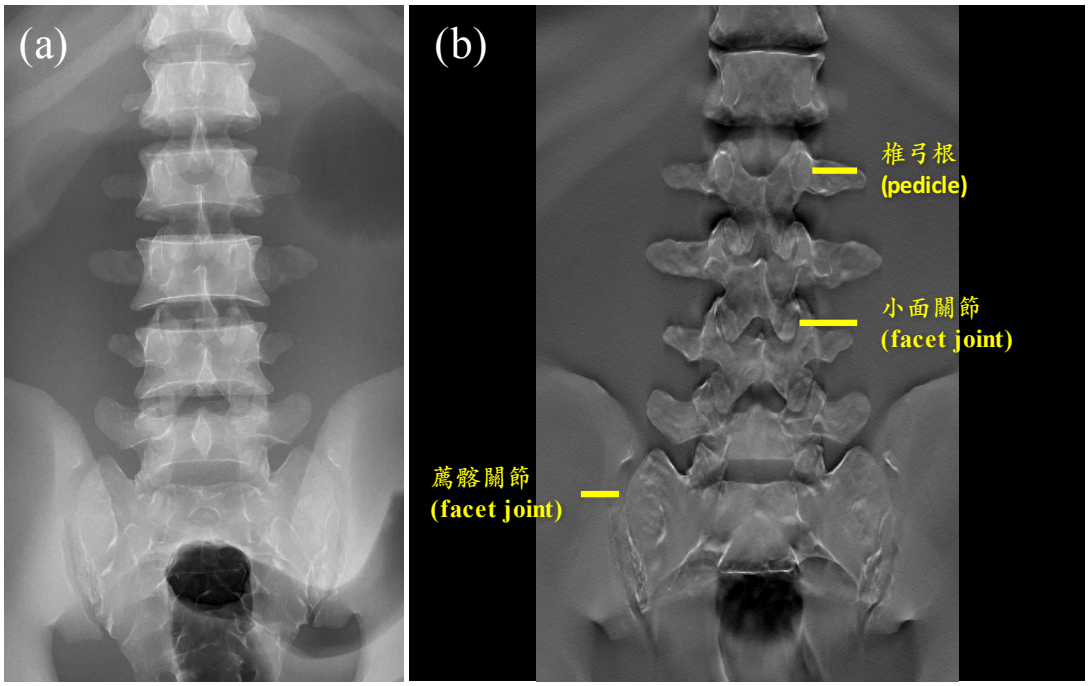

Figure 22: Phantom image (Spine AP view)

Figure 23 showed the lateral view of T-L spine tomosynthesis image. The tomosynthesis image (Figure 23 b) provides excellent image quality in cortical bone discrimination and image resolution compared with the conventional digital radiography (DR) (Figure 23 a). The spine detailed information at each depth could be visualized while the DR image showed the tissue superimposition and poor image resolution. The end plate, intervertebral foremen, vertebral body, and facet joint could be clearly visualized. The lateral view of spine tomosynthesis is very useful for orthopedic surgeon confirming the pre- and post-operative procedure and patient recovery condition after a surgery. The overall image contrast is good and the image artifact is acceptable and without impair in the diagnosis region.

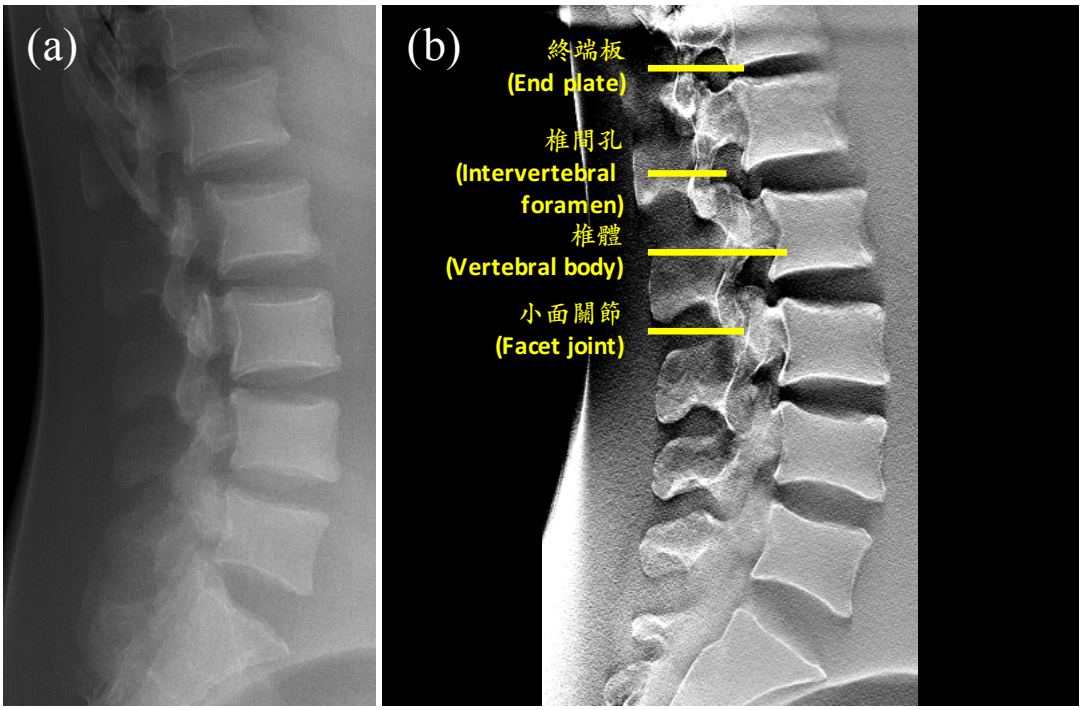

Figure 23: Phantom image (Spine Lateral view)

Figure 24 showed the AP view of foot tomosynthesis image. The tomosynthesis image (Figure 24 b) provides excellent image quality in bony structure discrimination and image resolution compared with the conventional digital radiography (DR) (Figure 24 a). The spine detailed information at each depth could be visualized while the DR image showed the tissue superimposition and poor image resolution. The talus bone, and calcaneus bone could be clearly visualized. The artificial bone fracture in tibia and fibula bone could be clearly discriminated.

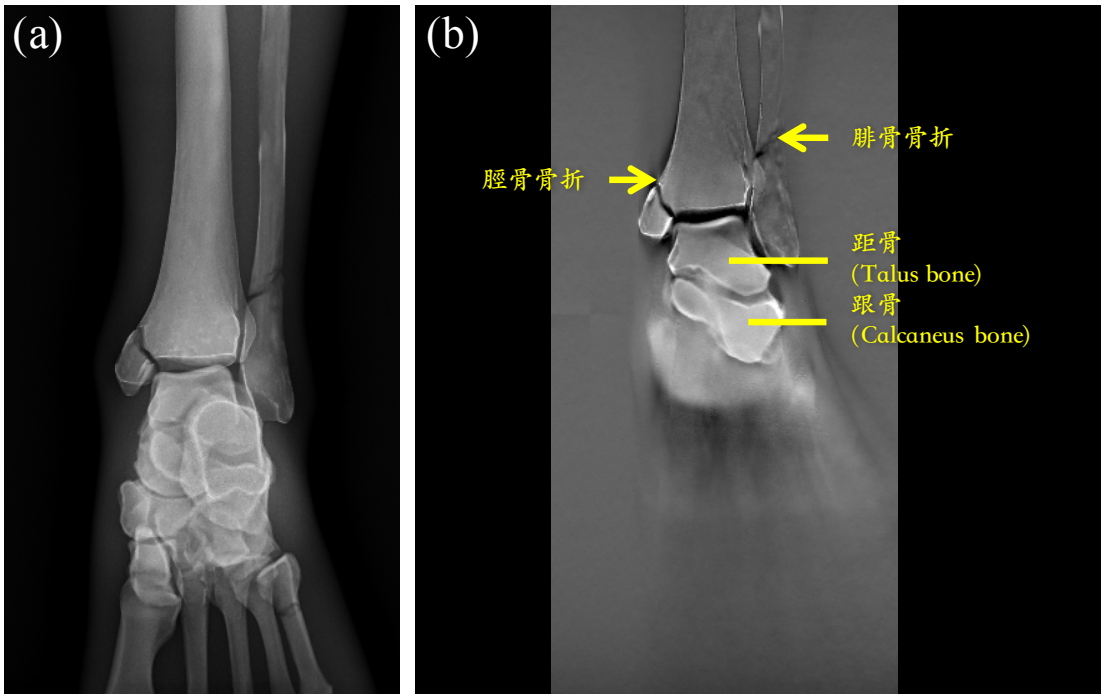

Figure 24: Phantom image (Ankle AP view)

Figure 25 showed the lateral view of foot tomosynthesis image. The tibia, calcaneus bone, cuboid bone, talus, and fourth metatarsal bone could be clearly visualized. The cortical bone could be clearly visualized in tomosynthesis image and its image contrast resolution is excellent. The overall image contrast is good and the image artifact is acceptable and without impair in the diagnosis region.

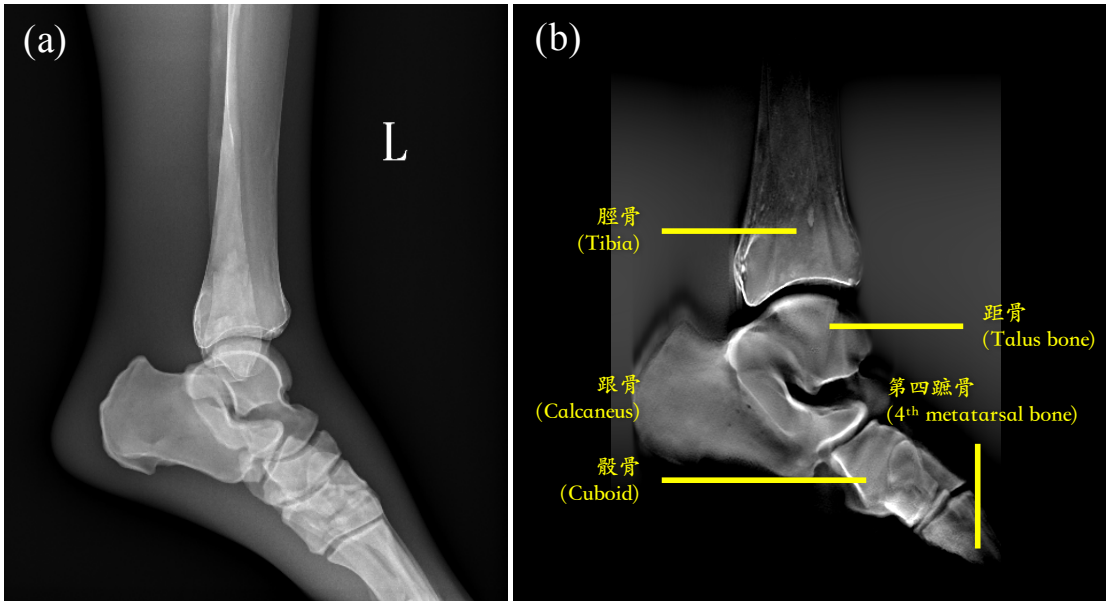

Figure 25: Phantom image (Ankle Lateral view)

Figure 26 showed the AP view of hand tomosynthesis image. The capitate, hamate, triquetrum, lunate, and scaphoid bones could be clearly visualized. The first trapezium fracture could be clearly visualized in tomosynthesis image and its image contrast resolution is excellent. The overall image contrast is good and the image artifact is acceptable and without impair in the diagnosis region.

In Simon et al study, he concluded that tomosynthesis has a higher sensitivity than radiography to detect bone erosions of the foot in patients with established rheumatoid Arthritis (RA) and imparts an almost equivalent radiation burden.

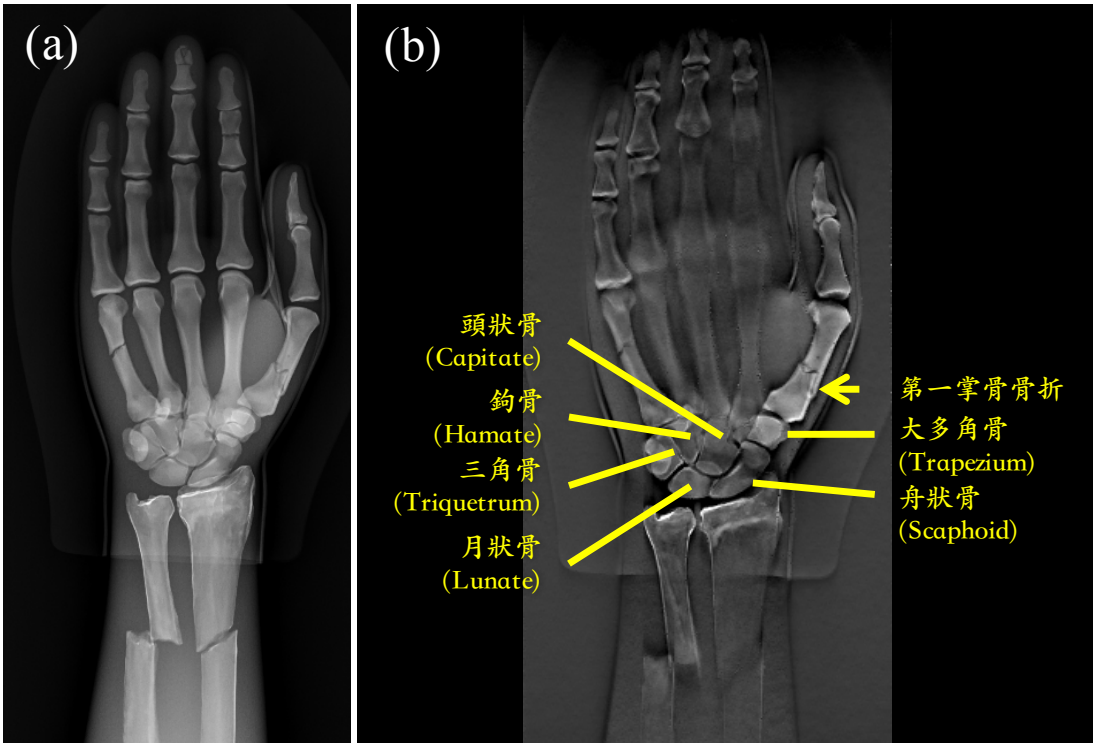

Figure 26: Phantom image (Hand AP view)

Figure 27 showed the lateral view of hand tomosynthesis image. The hamate bone, metacarpal bone, lunate bone, fourth distal phalange, middle phalange, and proximal phalange bones could be clearly visualized. The overall image contrast is good and the image artifact is acceptable and without impair in the diagnosis region.

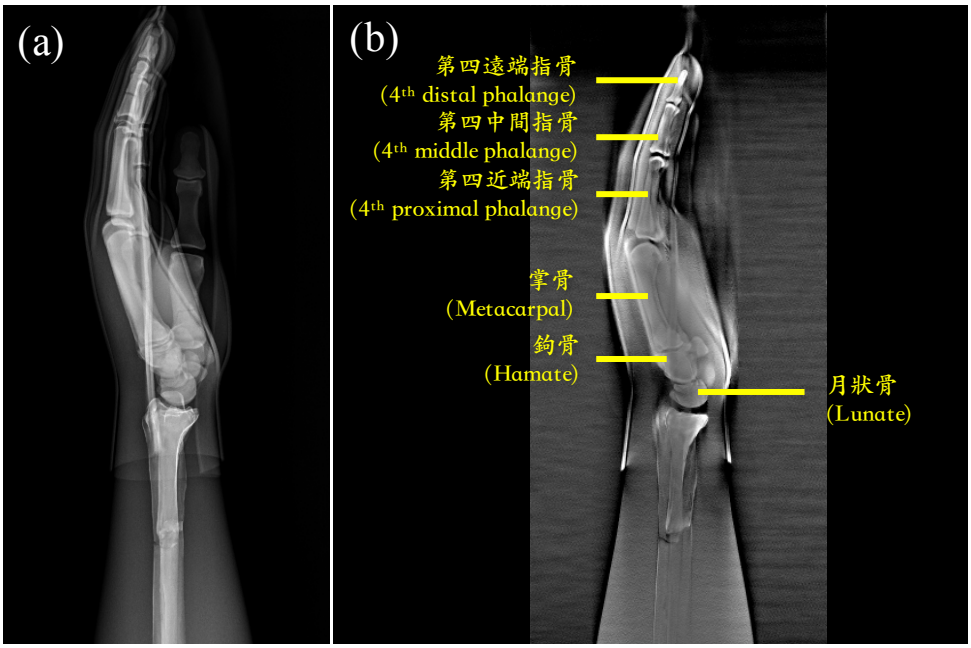

Figure 27: Phantom image (Hand Lateral view)

2. Phantom image quality analysis

Table 4 showed the phantom image noise distribution and its imaging parameters. All the images were randomized listed for ROI measurements and image quality qualitative analysis. The Image noise was 398 pixels and 125 pixels for Head AP and lateral view. The Image noise was 290 pixels for chest AP view. The Image noise was 330 pixels and 140 pixels for T-L spine AP and lateral view. The Image noise was 710 pixels and 297 pixels for Hand AP and lateral view. The Image noise was 401 pixels and 674 pixels for foot AP and lateral view. The radiation dose for X-ray tomosynthesis is lower than computed tomography (CT) examinations.

Table 4: Image noise distribution of phantom image for each protocol.

Protocol	**Head AP**	**Head Lateral**	**Chest AP**	**T-L spine AP**	**T-L spine Lateral**	**Hand AP**	**Hand Lateral**	**Foot AP**	**Foot Lateral**
Tube voltage (kVp)	87	87	120	80	80	57	57	70	70
Tube current (mA)	500	500	250	320	320	250	250	250	250
Exposure time (ms)	10	10	3.2	16	16	10	10	14	14
Angular range (deg)	±20	±20	±20	±20	±20	±20	±20	±20	±20
Number of projections	74	74	74	74	74	74	74	74	74
Center of depth (mm)	100	100	100	75	150	40	40	80	80
Source to detector distance (cm)	110	110	110	110	110	110	110	110	110
Reconstructed slice thickness (mm)	1	1	5	2	2	1	1	1	1
Reconstructed algorithm (SA, FBP)*	FBP	FBP	FBP	FBP	FBP	FBP	FBP	FBP	FBP
Image noise	**398**	**125**	**290**	**330**	**140**	**710**	**297**	**401**	**674**

Table 5: Qualitative diagnostic image quality with the five-grade method

Protocol	Head AP	Head Lateral	Chest AP	T-L Spine AP	T-L spine Lateral	Hand AP	Hand Lateral	Foot AP	Foot Lateral
Manufacture recommendation	5	5	5	5	5	5	5	5	5

The image noise and overall image quality acquired from the manufacture recommend protocol was acceptable for the radiologist. The image noise and overall image quality of adjusted protocols for lower the radiation dose or improvement of the image resolution from radiologist requirement was showed in Table 6. The image noise showed increase when the radiation dose was lowered. The overall diagnosis image quality still satisfied with the radiologist.

Table 6: Qualitative diagnostic image quality with the five-grade method for the adjusted protocols.

Protocol	Adjustment of imaging parameters	Image noise	Overall image quality
Head			
Adjustment 1	Reconstructed slice thickness 2 mm	348 (AP); 190 (lateral)	5
Chest			
Adjustment 1	Reconstruction algorithm of FBP, 100 kVp	302 (AP); 471 (lateral)	5
T-L Spine			
Adjustment 1	86 kVp, 500 mA, 2 ms		5
Hand			
Adjustment 1	50 kVp, 3.2 ms	252 (AP); 182 (lateral)	5
Adjustment 2 (AP view)	62 kVp	102	5
Foot			
Adjustment 1	60 kVp, 2.8 ms	158 (AP); 240 (lateral)	5
Adjustment 2	80 kVp	162 (AP); 445 (lateral)	5
Adjustment 3	60 kVp, 2.8 ms, reconstructed slice thickness 2 mm	146 (AP); 344 (lateral)	5
Adjustment 4	75 kVp	290 (AP); 463 (lateral)	5
Adjustment 5 (Lateral)	60 kVp, 2.8 ms, reconstructed slice thickness 2 mm	248	5

3. Organ dose and effective dose estimation

Table 7 showed the organ dose measurement in the phantom for the chest protocol. The effective dose was 0.883 mSv.

Table 7: Measured organ dose for the chest protocol.

Measured organs	**Organ dose (mGy)**
Esophagus	2.934
Lung	3.484
Stomach	0.472
Liver	1.788
Skin	0.451
Thyroid	3.359

4. Recommendation of IEC 60601-1-6 Usability

Table 8 showed the recommendation of the IEC 60601-1-6 usability. Item number one to ten are necessary function for every medical imaging facility. Each function should be established and labeled in the examination room. Beside the IEC report, the medical exposure modality should follow the regulation of Atomic Energy Council (AEC) in Taiwan.

Table 8: Recommendation of IEC 60601-1-6 Usability

Item no.	**operator-equipment interface**
1	markings and accompanying documents
2	Lights
3	Video displays
4	Push buttons
5	Touch screens
6	Auditory and visual information signals
7	ALARM signals
8	Vibratory signals
9	Keyboard and mouse
10	Haptic controls

4. Summary and conclusion

The project of Pre-clinical testing and usability assessment of TomoDR was completed by our research group. The diagnostic image quality for routine examinations (head, chest, spine, and and foot) using X-ray digital tomosynthesis was investigated. All the results indicated that the X-ray tomosynthesis can provide excellent image quality and detailed tomographic image resolution compared with conventional radiography. The recommendation of IEC 60601-1-6 usability was also provided in this report. Tomosynthesis could be an alternative for routine examination tool and superior to conventional radiography. We also suggested INER that clinical trial for patients undergo tomosynthesis should be further investigated in the future.

IV. References

1. Yuhara, T., Tamura, M., Ishikawa, T., Tate, E., Ueno, E., Nye, K., & Sabol, J. M. (2016). Whole-Body Clinical Applications of Digital Tomosynthesis. *Radiographics*, *36*(3), 735–750. http://doi.org/10.1148/rg.2016150184
2. Becker, A. S., Martini, K., Higashigaito, K., Guggenberger, R., Andreisek, G., & Frauenfelder, T. (2017). Dose reduction in tomosynthesis of the wrist. AJR Am J Roentgenol, 208(1), 159–164. http://doi.org/10.2214/AJR.16.16729
3. Clinical Experiences with Tomosynthesis in Orthopaedic Surgery at the Dokkyo Medical University Koshigaya Hospital. (2011). Clinical Experiences with Tomosynthesis in Orthopaedic Surgery at the Dokkyo Medical University Koshigaya Hospital, 1–2.
4. Quaia, E., Baratella, E., Cernic, S., Lorusso, A., Casagrande, F., Cioffi, V., & Cova, M. A. (2012). Analysis of the impact of digital tomosynthesis on the radiological investigation of patients with suspected pulmonary lesions on chest radiography. European Radiology, 22(9), 1912–1922. http://doi.org/10.1007/s00330-012-2440-3
5. Machida, H., Yuhara, T., Mori, T., Ueno, E., Moribe, Y., & Sabol, J. M. (2010). Optimizing parameters for flat-panel detector digital

tomosynthesis. Radiographics, 30(2), 549–562. http://doi.org/10.1148/rg.302095097

6. Gomi, T., Hirano, H., & Nakajim, M. (2012). X-Ray Digital Linear Tomosynthesis Imaging of Arthoroplasty. In Recent Advances in Arthroplasty. InTech. http://doi.org/10.5772/25746
7. Ha, A. S., Lee, A. Y., Hippe, D. S., Chou, S.-H. S., & Chew, F. S. (2015). Digital Tomosynthesis to Evaluate Fracture Healing: Prospective Comparison With Radiography and CT. American Journal of Roentgenology, 205(1), 136–141. http://doi.org/10.2214/AJR.14.13833
8. Simoni, P., Gérard, L., Kaiser, M.-J., Ribbens, C., Rinkin, C., Malaise, O., & Malaise, M. (2015). Use of Tomosynthesis for Detection of Bone Erosions of the Foot in Patients With Established Rheumatoid Arthritis: Comparison With Radiography and CT. American Journal of Roentgenology, 205(2), 364–370. http://doi.org/10.2214/AJR.14.14120
9. Xia, W., Yin, X.-R., Wu, J.-T., & Wu, H.-T. (2013). Comparative study of DTS and CT in the skeletal trauma imaging diagnosis evaluation and radiation dose. Eur J Radiol, 82(2), e76–e80. http://doi.org/10.1016/j.ejrad.2012.09.008
10. http://www.radtechonduty.com/2012/09/ap-projection-ankle.html
11. http://www.radtechonduty.com/2012/09/lateral-ankle-xray-rules.html
12. http://www.radtechonduty.com/2011/12/pa-projection-hand.html

13. https://radiopaedia.org/articles/hand-lateral-view-2
14. http://www.radtechonduty.com/2013/08/pa-projection-skull-series.html
15. https://www.meded.virginia.edu/courses/rad/cxr/technique3chest.html
16. http://www.radtechonduty.com/2014/09/ap-or-pa-projection-in-lumbar-spine-x.html